Strong Alignment Observed for the Time-Reversed Photoionization Process Studied in Relativistic Collisions with Bare Uranium Ions

Th. Stöhlker,[1,2] F. Bosch,[2] A. Gallus,[2] C. Kozhuharov,[2] G. Menzel,[2] P. H. Mokler,[2] H. T. Prinz,[2] J. Eichler,[3] A. Ichihara,[4] T. Shirai,[4] R. W. Dunford,[5] T. Ludziejewski,[6] P. Rymuza,[6] Z. Stachura,[7] P. Swiat,[8] and A. Warczak[8]

[1]*Institut für Kernphysik, University of Frankfurt, 60486 Frankfurt, Germany*
[2]*Gesellschaft für Schwerionenforschung, 64220 Darmstadt, Germany*
[3]*Bereich Theoretische Physik, Hahn-Meitner-Institut Berlin, 14109 Berlin, Germany, and Fachbereich Physik, Freie Universität Berlin, 14195 Berlin, Germany*
[4]*Japan Atomic Energy Research Institute, Tokai-mura, Ibaraki 319-11, Japan*
[5]*Physics Divison, Argonne National Laboratory, Argonne, Illinois 60439*
[6]*Institute for Nuclear Studies, 05-400 Świerk, Poland*
[7]*Institute of Nuclear Physics, 31-342 Cracow, Poland*
[8]*Institute of Physics, Jagiellonian University, 30-059 Cracow, Poland*

(Received 3 July 1997)

In high-energy atomic collisions between bare high-Z projectiles and low-Z target atoms, an electron may be captured radiatively into an excited projectile state which subsequently decays by x-ray emission. This process is the inverse of two-photon–one-electron ionization, in which the first photon resonantly excites an electron from the hydrogenic $1s_{1/2}$ ground state and a second photon ionizes the excited electron. We present an experimental and theoretical study of the angular distribution of the Ly-α_1 ($2p_{3/2} \rightarrow 1s_{1/2}$) x rays following radiative electron capture. From the observed anisotropic emission pattern a significant alignment of the intermediate $2p_{3/2}$ state is deduced. [S0031-9007(97)04327-5]

PACS numbers: 34.70.+e

Recent experimental studies of inner-shell photoionization have stressed the role of relativistic effects and higher transition multipoles beyond the electric-dipole approximation [1]. Sensitivity to such effects is enhanced by measurement of angular distributions rather than angle integrated cross sections [2]. Interestingly, information on these higher-order effects in the photoionization of inner shells of very heavy atoms can also be obtained through measurements of angular distributions of photons emitted following radiative electron capture (REC) into excited states of highly charged ions. For the case of the heaviest atoms, REC into bare ions provides the only experimental access for photoionization studies in the absence of electron screening corrections.

With present-day accelerators, it is possible to produce relativistic beams of bare high-Z ions like U^{92+} and Pb^{82+} [3,4]. If a high-Z ion collides with a low-Z target atom, it may capture an electron radiatively, that is, with the simultaneous emission of a photon, which carries away the excess energy and momentum. Since the loosely bound target electrons can be considered as quasifree, REC is essentially the inverse of the photoelectric effect [5,6]. If REC occurs into an excited state, say the $2p_{3/2}$ level, this state decays into the $1s_{1/2}$ ground state by emitting a Lyman-α_1 photon. For high-Z projectiles and low-Z targets nonradiative capture plays no role [7]; hence the detection of a decay photon in coincidence with the down-charged projectile is a clear indication of a two (or more)-photon process. This reaction is the inverse of an otherwise unobservable high-energy two-photon–one-electron ionization: Initially, a photon resonantly excites the hydrogenic $2p_{3/2}$ state from the $1s_{1/2}$ ground state, and, subsequently, another photon ionizes the excited electron within the lifetime of the $2p_{3/2}$ state, i.e., a time of the order of 10^{-17} s. In this Letter, we are interested in the magnetic subshell population produced by REC into the $2p_{3/2}$ state. This provides us with detailed information on the dynamics of the photoionization process for a high-Z one-electron ion, in which the electron-photon interaction is governed by relativistic effects. Information on the population of magnetic substates is obtained either from the angular distribution of the emitted photons [10] or from polarization measurements [8]. However, in the present case, the Ly-α_1 transition energy is close to 100 keV, so that the photon polarization is almost impossible to detect and hence the alignment of the $2p_{3/2}$ state can be deduced only from an angular distribution measurement.

Here, we report the first experimental study of the photon angular distribution of the Lyman-α_1 radiation following radiative electron capture into the $2p_{3/2}$ level of H-like uranium. This allows us to obtain magnetic-substate sensitive information on the REC process under uniquely clean experimental conditions. We emphasize that alignment studies following electron capture into inner shells of high-Z atoms are very scarce and according to our knowledge no such data exist for relativistic collision systems. Only for the different process of resonant transfer and excitation an alignment study has been reported for high-Z ions [11].

 0031-9007/97/79(17)/3270(4)$10.00

For a theoretical description of REC followed by radiative deexcitation [9], we have to consider a second-order process with the following sequence of events: In the first step, a quasifree electron with asymptotic momentum $\mathbf{p}$ and spin projection s, interacting with the Coulomb field of the projectile, is captured into an excited state n with angular momentum j_n and projection μ_n, while at the same time a photon with wave vector $\mathbf{k}$ and helicity $\lambda = \pm 1$ is emitted. In the second step, the state n decays into the lower state i (with j_i, μ_i) by emitting another photon with wave vector $\mathbf{k}'$ and helicity $\lambda' = \pm 1$. Both steps are separated in time, because the collision time is about 1000 times shorter than the half-life of the $2p_{3/2}$ state. Equivalently, we consider the time-reversed process of photoionization. The absorption of the photon $\mathbf{k}'$, λ' excites the initial state i to the intermediate state n. Subsequently, the electron in state n is ionized by the photon $\mathbf{k}$, λ into a Coulomb-distorted continuum state $\mathbf{p}$, s with respect to the projectile. Since the REC photon is not observed, one has to integrate over $\hat{\mathbf{k}} = \mathbf{k}/k$ and to sum over λ. Since angular momentum projections and polarizations are usually not detected, we also have to sum incoherently over μ_i, s, and λ'.

We are interested in angular distributions and, hence, in the following, ignore angle-independent common factors. The angular correlation in the projectile frame is given by

$$W \propto \sum_{\lambda,\lambda'} \sum_{\mu_i} \sum_{s} \int d\hat{\mathbf{k}} \left| \sum_{\mu_n} \langle \mathbf{p}, s\, | \boldsymbol{\alpha} \cdot \hat{\mathbf{u}}_{\lambda} e^{i\mathbf{k}\cdot\mathbf{r}} | j_n \mu_n \rangle \times \langle j_n \mu_n | \boldsymbol{\alpha} \cdot \hat{\mathbf{u}}_{\lambda'} e^{i\mathbf{k}'\cdot\mathbf{r}} | j_i \mu_i \rangle \right|^2, \quad (1)$$

where $\boldsymbol{\alpha}$ is the vector formed from the Dirac matrices and $\hat{\mathbf{u}}_{\lambda,\lambda'}$ are the unit vectors for the circular polarization of the x rays. For the "final" electron state, exact hydrogenic continuum wave functions with respect to the projectile are adopted [5], which are given by a partial-wave expansion in terms of spherical states characterized by the Dirac quantum number $\kappa(j, l)$ and the projection μ. The plane photon waves $\exp(i\mathbf{k}\cdot\mathbf{r})$ are expanded in terms of multipoles. For the transition from the initial state $i = 1s_{1/2}$ to the intermediate state $n = 2p_{3/2}$, only the electric dipole term contributes. Performing the spinor and angular momentum algebra, carrying out the summations and integrations occurring in Eq. (1) and calculating the exact radial matrix elements numerically [5], one obtains the angular correlation in the form

$$W(\theta) = A_0 + A_2 P_2(\cos\theta) \propto 1 + \beta_{20}(1 - \tfrac{3}{2}\sin^2\theta). \quad (2)$$

Here θ is the angle between the direction $\hat{\mathbf{k}}'$ of the deexcitation photon and the asymptotic direction $\hat{\mathbf{p}}$ of the electron while P_2 is the second-order Legendre polynomial. The angular correlation is completely determined by the anisotropy coefficient β_{20}. $W(\theta)$ is symmetric about 90° in the projectile frame and specifically isotropic if the intermediate state has $j_n = \frac{1}{2}$ as is the case for the Ly-α_2 ($2p_{1/2} \rightarrow 1s_{1/2}$) transition. We may also calculate β_{20} from the alignment $\mathcal{A}_2$ of the state n (cf. e.g., [10]) defined as

$$\mathcal{A}_2 = \frac{\sigma(\frac{3}{2}, \pm\frac{3}{2}) - \sigma(\frac{3}{2}, \pm\frac{1}{2})}{\sigma(\frac{3}{2}, \pm\frac{3}{2}) + \sigma(\frac{3}{2}, \pm\frac{1}{2})} = \frac{1}{\alpha}\,\beta_{20}, \quad (3)$$

where $\sigma(j_n, \mu_n)$ is the population of the magnetic substate μ_n. For the $2p_{3/2} \rightarrow 1s_{1/2}$ transition, $\alpha = \frac{1}{2}$ [10].

After transformation to the laboratory frame, the differential Ly-α_1 production cross section has the general form [9]

$$\frac{d\sigma_{\text{Ly-}\alpha_1}(\theta_{\text{lab}})}{d\Omega_{\text{lab}}} \propto \frac{1}{\gamma^2(1 - \beta\cos\theta_{\text{lab}})^2}\left[1 + \beta_{20}\left(1 - \frac{3}{2}\,\frac{\sin^2\theta_{\text{lab}}}{\gamma^2(1 - \beta\cos\theta_{\text{lab}})^2}\right)\right], \quad (4)$$

where $\beta = v/c$ and $\gamma = 1/\sqrt{1 - \beta^2}$ (v denotes the projectile velocity and c the speed of light). Note that due to the Lorentz transformation to the laboratory system, the maximum of the distribution is located at a forward observation angle of $\cos\theta_{\text{lab}} = \beta$.

Experimental data for the anisotropy parameter β_{20} were taken for bare Pb^{82+} and U^{92+} ions at the gas-jet target of the ESR storage ring at GSI-Darmstdt [12]. Characteristic projectile x rays were produced by radiative electron capture from the gas-jet target into the bare, fast moving projectiles. The photons were always registered by x-ray detectors in coincidence with the down-charged projectiles (for a detailed description of the experimental setup used, refer to Ref. [13]). In most of the experiments, the gas-jet target area was surrounded by four Ge(i) detectors with thicknesses of 12 or 15 mm, mounted at observation angles of 48°, 90°, and 132°. The detectors installed at 48° and 132° were separated from the ultrahigh vacuum of the ESR beam line by 150 μm thick Be windows whereas at 90° a 50 μm thick stainless steel window was used. At 48°, two detectors were installed symmetrically on opposite sides of the reaction chamber. One detector at 48° and one at 90° consisted of seven equidistant, parallel segments, each furnished with a separate readout. At all of the observation angles, the x-ray detector/target geometry chosen made it possible to resolve the splitting of the Ly-α transitions into the Ly-α_1 and Ly-α_2 components. These lines are separated in the projectile frame by 2.8 keV for H-like lead and by 4.5 keV for H-like uranium. Note that the Ly-α_2 component for such high-Z ions is blended with the fast $2s_{1/2} \rightarrow 1s_{1/2}$ **M1** transition.

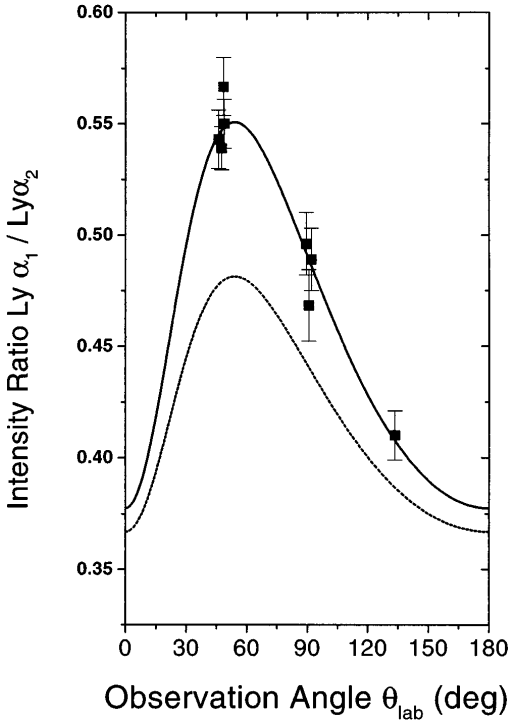

FIG. 1. Experimental Ly-α_1/Ly-α_2 intensity ratio (solid squares) measured for 220 MeV/u $U^{92+} \rightarrow N_2$ collisions. The solid line depicts the result of the least squares adjustment of Eq. (4) to the experimental data.

The experimental anisotropy parameters were determined by normalizing the intensity of the investigated Ly-α_1 transition to that of the Ly-α_2 (+**M1**) radiation. Since the latter is isotropic in the projectile frame and energetically close to the Ly-α_1 line, this method allows us to strongly reduce the influence of possible systematic uncertainties. Note that the factor preceding the square bracket in Eq. (4), which describes the transformation of the solid angle, cancels for the line intensity ratio. The total number of counts of the individual Ly-α transitions was obtained by integration of theoretical line shapes (Gaussian distributions convoluted with rectangular profiles in order to account for the Doppler broadening) which were fitted to the Ly-α transitions appearing in the spectra. Finally, the anisotropy parameter β_{20} for each experiment was deduced from a least squares adjustment of Eq. (4) to the experimental Ly-α_1/Ly-α_2 intensity ratios. For this purpose, β_{20} and a constant multiplying the square brackets of Eq. (4) were treated as free fit parameters. As an example, the Ly-α intensity ratios (full squares) measured for 220 MeV/u $U^{92+} \rightarrow N_2$ collisions are given in Fig. 1 as a function of the laboratory observation angle θ_{lab} (the data measured by the segmented x-ray detectors were combined into three sets for each detector in order to improve counting statistics). As can be seen from Fig. 1, the experimental data show a strong anisotropy for the $2p_{3/2}$ ground-state transition which is well reproduced by a fit to Eq. (4) (see solid line in Fig. 1). In Table I, we display the experimental and theoretical anisotropy parameters β_{20} of the Ly-α_1 radiation obtained for the various collision systems studied. The calculations for *L*-REC are based on rigorous electronic wave functions [5,6]. The same is true for the cross sections of REC into the sublevels of the *M* and *N* shells which are needed in order to consider also cascade feeding of the *L*-subshell levels. For the latter purpose, REC into highly excited levels up to $n = 20$ was also taken into account by applying the $1/n^3$ scaling law, valid at high energies [3]. For the cascade calculations, the required transition rates were taken from the GRASP code [14]. The effect of cascade feeding is already included in the theoretical predictions presented in Table I. In parentheses, we give the values without cascade feeding. Since it is known [13,15] that the dipole approximation (fortuitously) provides a good approximation to the total cross section but is not suitable for REC angular distributions, it is of interest to examine its performance for the angular correlations studied here. In the last column, we therefore give the anisotropies calculated in the dipole approximation to the REC process, which leads to a coherent superposition of continuum $s_{1/2}$, $d_{3/2}$, and $d_{5/2}$ states for the captured electron. Since all wave functions involved are exact, the length form (with the operator $\mathbf{r}$) and the velocity form (with the operator $\boldsymbol{\alpha}$) are found to yield identical results. However, we emphasize that the convergence of the cross section requires partial waves up to $|\kappa| = 15$. As seen from Table I, both the experimental and the theoretical results exhibit a significant alignment with negative anisotropy parameters β_{20}. This means that REC into the $2p_{3/2}$ level populates

TABLE I. Experimental anisotropy parameters β_{20} of the Ly-α_1 radiation obtained for the various collision systems studied. The theoretical results are given for a full partial-wave expansion of the continuum and for dipole transitions into the $s_{1/2}$, $d_{3/2}$, and $d_{5/2}$ states. Both cases include the feeding transitions from higher excited levels, while the values in parentheses represent the anisotropy from REC into the $2p_{3/2}$ state alone.

Collision	System	Experiment	Theory	Dipole approx.
277 MeV/u	$Pb^{82+} \rightarrow N_2$	-0.26 ± 0.08	-0.135 (-0.241)	-0.155 (-0.277)
220 MeV/u	$U^{92+} \rightarrow N_2$	-0.23 ± 0.02	-0.172 (-0.284)	-0.209 (-0.345)
295 MeV/u	$U^{92+} \rightarrow N_2$	-0.27 ± 0.09	-0.161 (-0.271)	-0.197 (-0.331)
358 MeV/u	$U^{92+} \rightarrow N_2$	-0.18 ± 0.03	-0.150 (-0.264)	-0.184 (-0.322)
358 MeV/u	$U^{92+} \rightarrow CH_4$	-0.21 ± 0.04	-0.150 (-0.264)	-0.184 (-0.322)

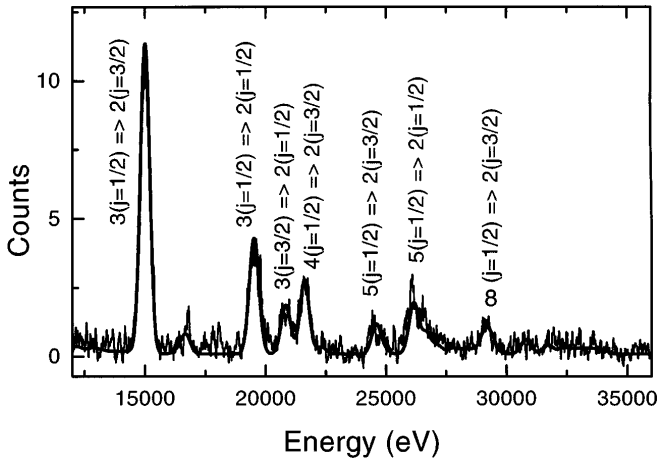

FIG. 2. Balmer spectrum (emitter system) of H-like uranium measured in coincidence with electron capture for $U^{92+} \rightarrow N_2$ collisions at 358 MeV/u. The solid line gives the result of a cascade calculation using the theoretical REC cross sections.

especially the magnetic $\mu_n = \pm\frac{1}{2}$ sublevels and leads to emission of strongly polarized Ly-α_1 photons. It also implies that the emission of Ly-α_1 photons occurs preferentially perpendicular to the beam direction. Moreover, the alignment seems to slightly increase with decreasing collision energy. Although there is qualitative agreement between the experimental and theoretical results, the experimental anisotropy values are systematically larger than those obtained using the complete theoretical treatment. In contrast, the dipole approximation, which certainly is inadequate for the collision systems discussed, appears to be in closer agreement with the experimental findings. In this context, the cascade feeding of the $2p_{3/2}$ level is of great importance since it leads to a considerable reduction of the theoretical alignment (see values given in the Table I). Here, it is important to note that the cascade feeding contribution relative to REC into the $2p_{3/2}$ state was also determined experimentally by detection of the Balmer radiation ($n = 3, 4, 5, \ldots \rightarrow n = 2$ transitions). In Fig. 2 we compare the experimental Balmer spectrum measured at 48° for $U^{92+} \rightarrow N_2$ collisions at 358 MeV/u with a simulation of the spectrum based on the cascade feeding calculations. For comparison, the dominant transition line appearing at an x-ray energy of 15 keV was used to normalize the experimental Balmer spectrum ($3s_{1/2} \rightarrow 2p_{3/2}$ transitions; see level assignment given in the figure). As displayed in Fig. 2, all prominent lines in the spectrum were identified as transitions originating from states with $j = \frac{1}{2}$ which confirms that no alignment is introduced by cascades. The latter contributes about 40% to the total Ly-α_1 emission cross section.

In conclusion, we completed the first experimental study of the magnetic-substate population for the time-reversed photoionization process in ion-atom collisions. The measured angular distribution of the Ly-α_1 radiation following REC into the $2p_{3/2}$ state of high-Z projectiles at relativistic energies (ranging from 220 up to 358 MeV/u) yields a significant negative value of the alignment parameter. It shows that REC into $2p_{3/2}$ level populates mostly the $\mu_n = \pm\frac{1}{2}$ magnetic sublevels (by about 75%), which implies that the Ly-α_1 radiation is strongly linearly polarized (+38% to +40%). The intense Balmer radiation observed proves that the cascade feeding of the $2p_{3/2}$ level, which leads to isotropic x-ray emission, must be taken into account. Therefore, the alignment created by direct radiative capture into the $2p_{3/2}$ state is larger than that deduced from the Ly-α_1 emission leading to our conclusion that REC *almost exclusively* populates the $\mu_n = \pm 1/2$ substates. We have to emphasize, that to our knowledge, no other process has been identified in fast ion-atom or electron-ion collisions in which such a strong alignment occurs.

One of us (R. W. D.) is supported by GSI and by U.S. DOE under Contract No. W-31-109-ENG-38. Three of us (Z. S., P. S., A. W.) were supported by GSI and by the Polish Committee for Scientific Research (KBN) under research Grants No. 2P03B10910 and No. C/002/97.

[1] B. Krässig *et al.*, Phys. Rev. Lett. **75**, 4736 (1995).
[2] A. F. Starace, in *Corpuscles and Radiation in Matter*, edited by W. Mehlhorn, Handbuch der Physik Vol. 31 (Springer-Verlag, Berlin, 1982), p. 1.
[3] See, e.g., J. Eichler and W. E. Meyerhof, *Relativistic Atomic Collisions* (Academic Press, San Diego, 1995).
[4] P. H. Mokler and Th. Stöhlker, Adv. At. Mol. Opt. Phys. **37**, 297 (1996).
[5] A. Ichihara, T. Shirai, and J. Eichler, Phys. Rev. A **49**, 1875 (1994).
[6] J. Eichler, A. Ichihara, and T. Shirai, Phys. Rev. A **51**, 3027 (1995).
[7] Th. Stöhlker *et al.*, Nucl. Instrum. Methods Phys. Res., Sect. B **87**, 64 (1994).
[8] E. Takacs *et al.*, Phys. Rev. A **54**, 1342 (1996).
[9] J. Eichler, Nucl. Phys. **A572**, 147 (1994).
[10] E. G. Berezhko and N. M. Kabachnik, J. Phys. B **10**, 2467 (1977).
[11] T. Kandler *et al.*, Phys. Lett. A **204**, 274 (1995).
[12] Th. Stöhlker *et al.*, Phys. Rev. Lett. **71**, 2184 (1993).
[13] Th. Stöhlker *et al.*, Phys. Rev. A **51**, 2098 (1995).
[14] K. Dyall *et al.*, Comput. Phys. Commun. **55**, 425 (1989).
[15] A. Ron *et al.*, Phys. Rev. A **50**, 1312 (1994).